Polymer Journal (2018) 50:251–260
https://doi.org/10.1038/s41428-017-0008-4

ORIGINAL ARTICLE

Producing a magnetically anisotropic soft material: synthesis of iron oxide nanoparticles in a carrageenan/PVA matrix and stretching of the hybrid gelatinous bulk

Rie Sakai[1] · Yoshikuni Teramoto[2,3] · Yoshiyuki Nishio[1]

Received: 7 September 2017 / Revised: 13 October 2017 / Accepted: 22 October 2017 / Published online: 22 December 2017
© The Society of Polymer Science, Japan 2018

Abstract

We propose a method for preparing magnetically anisotropic soft materials that includes chemical loading (in situ synthesis) of iron oxide nanoparticles in a matrix composed of κ-carrageenan (Car) and poly(vinyl alcohol) (PVA) followed by mechanical stretching of the hybrid in a wet process. Anionic Car was used to accommodate the iron oxide nanoparticles and was blended in advance with PVA, which has the ability of high orientation. Scanning electron microscopy revealed that the loaded granular iron oxide nanoparticles (50–100 nm) formed elliptical clusters upon stretching of the hybrid composite. Wide-angle X-ray diffraction measurements indicated that the PVA constituent was oriented in the draw direction. With the orientation of the composite matrix, the incorporated iron oxide nanoparticles gathered to form elliptical clusters. The drawn samples showed different amplitudes in the magnetization ($M_{\parallel} > M_{\perp}$) when measured in two setups in which the applied field was parallel (∥) or perpendicular (⊥) to the draw direction. The specific responses of the drawn sheets to an external magnetic stimulus were visualized and were reasonably attributed to an effect of the magnetic anisotropy created by the preferred orientation of the nanoparticle aggregates.

Introduction

Magnetic nanocomposites of eco-friendly or biocompatible polysaccharides [1–21] have potential for use in various applications. The possible applications include green filtration and separation systems, information transfer and storage media, fabrics for electromagnetic wave shielding, field-sensitive actuators and sensors, magnetic drug-delivery systems, and other biomedical products.

We have reported a series of studies in which iron ions were chelated to anionic polysaccharides and then oxidized in situ via $Fe(OH)_2$ production to form iron oxide nanoparticles [9, 12, 17, 21]. We previously established conditions for regulating the amount and size of the magnetic iron oxide nanoparticles; therefore, it was possible to obtain hybrids containing superparamagnetic (SPM) iron oxide particles of several tens of nanometers. For instance, by repeating the in situ synthetic cycle three–four times within a carrageenan (Car) matrix, magnetic composites that possessed a high saturation magnetization (M_s) reaching ~25 emu/g sample at 298 K were easily obtained without impairing the SPM character [17].

In a recent study using a combination of cellulose nanocrystals (CNCs) and Car as the matrix, we reported that the iron oxide-containing nanocomposites exhibited "shape magnetic anisotropy" after an appropriate treatment to array the magnetic nanoparticles [21]. The concept of material design was based on the following idea: the magnetic iron oxide nanoparticles were synthesized in situ in the CNC/Car matrix; the nanocomposites obtained in sheet form were subjected to a drawing process to induce a specific orientation; thus, the distance between magnetic nanoparticles, which were originally finely dispersed, decreased enough to allow the magnetic walls to move even though completely separate magnetic domains were present before the orientation treatment. The resulting spheroidal clusters approximately behaved as ferromagnets, although the original magnetic nanoparticles themselves were isotropic granules

✉ Yoshikuni Teramoto
teramoto@gifu-u.ac.jp

[1] Division of Forest and Biomaterials Science, Graduate School of Agriculture, Kyoto University, Kyoto 606-8502, Japan

[2] Department of Applied Life Science, Faculty of Applied Biological Sciences, Gifu University, Gifu 501-1193, Japan

[3] Center for Highly Advanced Integration of Nano and Life Sciences (G-CHAIN), Gifu University, Gifu 501-1193, Japan

and imparted SPM properties [21]. Eventually, different amplitudes of a demagnetizing field were induced inside the nanocomposite samples by varying with the external magnetic vector, and macroscopic anisotropic magnetization was accomplished.

In the present study, we propose a simpler method for preparing nanocomposites with magnetic anisotropy. For this purpose, Car (κ-type) was blended with poly(vinyl alcohol) (PVA) and used as a matrix. Both the component polymers are supplied as general industrial raw materials. The microcomposition can be done in a simple process of mixing Car and PVA aqueous solutions. For this combination, the compatibility was evaluated based on the melting point depression of the PVA component [22]. Recently, an attempt was made to prepare Car/PVA composites as adsorbents for cationic dyes; magnetite nanoparticles were incorporated into the composites to easily recover the absorbent with a magnet [23]. On the other hand, here, we expect that Car possessing sulfo groups is a necessary component for intercalating iron ions to produce magnetic iron oxide, while the PVA constituent allows the entire matrix to stretch to provide an anisotropically aggregated array structure of iron oxide particles. The microcrystals and hydrogen bonding interactions of PVA behave as cross-linking points, so it is assumed that high deformation of the entire matrix, including the amorphous regions, is possible. For PVA gel alone, it was impossible to effectively incorporate iron oxide by this in situ method [9]. Meanwhile, it is difficult to dramatically deform the matrix of κ-type Car, which gives elastic gels [24, 25]. The combination of Car and PVA is thus useful.

To demonstrate this concept, we first examined the compatibility of Car and PVA based on the glass transition behavior determined by differential scanning calorimetry (DSC). After that, magnetic iron oxide was synthesized in situ in the composite matrix in a manner similar to that of our previous studies. We sought to optimize the process of stretching the gel-like nanocomposites containing iron oxide nanoparticles. The nanocomposites were then subjected to wide-angle X-ray diffraction and morphological observations to characterize the orientation behavior of the composites and the distribution of iron oxide nanoparticles. The magnetic anisotropy was evaluated with a superconducting quantum interference device (SQUID). We also demonstrated several patterns of anisotropic response of the products to external magnetic stimuli.

Experimental procedures

Original materials

The carbohydrate polymer sample of Car was a commercial product of κ-carrageenan (CP Kelco ApS (Lille Skensved, Denmark), GENUGEL WR-78-J, lot no. 035400), and the molecular weight and sulfur content (S) were determined in the preceding study as follows: [17] $M_w = 8.28 \times 10^5$, $M_w/M_n = 2.21$, and S = 5.97 wt%. PVA was supplied as PVA-HC by Kuraray Co.; the nominal degree of polymerization was 1750, and the saponification value was 99.9 mol%.

Ferrous chloride tetrahydrate ($FeCl_2 \cdot 4H_2O$) and H_2O_2 aqueous solutions were obtained from Wako Pure Chemical Ind., Ltd., and all other chemicals and solvents used were guaranteed reagent grade and employed without further purification. However, the water (usually distilled) and ethanol involved in the synthesis of iron oxides in the polymer composite gels were degassed by bubbling N_2 through them prior to use.

Iron oxide incorporation into Car/PVA gels

Aqueous solutions of Car and PVA were prepared separately at concentrations of 5.0 and 10 wt%, respectively, by dissolving the original polymer materials in water at 95 °C under continuous stirring. The solutions were mixed at 95 °C such that the solid weight ratio of Car/PVA was 20/80, and the mixture was stirred for 30 min at that temperature. The Car/PVA weight ratio (20/80) was adopted in consideration of the stretchability of the composite (see later discussion). The hot mixture was poured into a rectangular Teflon tray and transformed into a hydrogel by cooling naturally to room temperature (23 °C).

The Car/PVA gel was then immersed in an excess of an ethanol/water mixture (23 °C) containing $FeCl_2$ at a concentration of 0.10 M. The ethanol/water mixture used in this study was prepared by mixing the two solvents in a volume ratio of 1:1. After immersion in the salt solution for 2 h, the Fe^{2+}-intercalated gel was lightly washed with ethanol/water and soaked in a 1.0 M NaOH solution in ethanol/water (pH ≈13) for 2 h to produce ferrous hydroxide in the polymer composite network. The entire system (300 mL flask) was heated to 65 °C, and a 2.0 wt% H_2O_2 solution in ethanol/water was added dropwise into the alkaline medium over a period of 15 min. The oxidized gel (dark red–brown color) was removed from the container and washed with ethanol/water. The gel samples oxidized one time by this method were further oxidized in two subsequent cycles involving ferrous ion intercalation, alkali treatment, and oxidization with hydrogen peroxide. The sequence of the procedures for the in situ synthesis of iron oxide in the gel

matrix was similar to that applied in the preparation of PVA-free carrageenan gels in the preceding study [17]. A portion of the respective gel products (Car/PVA/Fe) was cut away and stored in a refrigerator until use for magnetometry measurements, and the rest of the sample was utilized in the step for preparing drawn sheets.

Preparation of drawn sheets of Car/PVA/Fe

An iron oxide-containing gel sample with a moisture content of ~90 wt% was cut into small pieces and placed in a 50-mL beaker. The beaker was placed in a water bath at 65 °C, and the sample in the beaker was stirred with a glass rod to facilitate its transition to the sol state. The sol sample was transferred to a micropipette and then discharged from the pipette into *t*-butyl alcohol (*t*-BuOH) (30 °C) stirred at 800 rpm. The stirring was continued for 10 min. Thereafter, the resulting fibrous, cylindrical samples were removed from the *t*-BuOH, and the wet samples were each stretched to ~four times their original lengths using tweezers in the air at 23 °C. The samples after stretching had a diameter of 1.8 mm and were cut to 12 mm lengths. The stretched sample was fixed on a glass slide with adhesive tape, air- and vacuum-dried, and then subjected to subsequent measurements. Even though the wet sample had the form of a fibrous cylinder, the sample after drying became a sheet with a smooth surface and a size of 12 mm long, 2 mm wide, and 0.45 mm thick. Similarly, sheet samples from the as-spun state were also prepared. The diameter immediately after extrusion from the micropipette was ~5 mm, and after drying with the ends fixed, the sample became a sheet with a width of 5.5 mm and a thickness of ~1 mm.

Measurements

DSC was conducted for the Car/PVA composites with different weight ratios on a Hitachi High-Tech Science Corporation DSC6200/EXSTAR6000 apparatus. The measurements were performed on 7-mg samples under a nitrogen atmosphere after calibrating the temperature readings with an indium standard. The samples were first heated to 250 °C and immediately quenched to −140 °C. Then, the second scans were collected from −140 °C to 260 °C to record stable thermograms. The glass transition temperature (T_g) was determined from the midpoint of the discontinuity in the heat flow.

The content of iron in the Car/PVA/Fe composite was measured by a redox titration method similar to that previously reported [17].

Magnetometry measurements were carried out on air-dried sheet samples 2 mm wide and 5 mm long with a superconducting quantum interference device (SQUID), MPMS-5 from Quantum Design Inc. The applied magnetic field (H) was varied through a cycle of 0 T → 5 T → −0.1 T → 0 T at a constant temperature. For a given sample, the magnetization (M) vs. H data were collected at 298 and 100 K. With regard to the drawn sheets, the draw direction (DD, the major axis of the specimens in this case) was set parallel (∥) or perpendicular (⊥) to the applied field; thus, two definable magnetizations, $M_{\parallel}$ and $M_{\perp}$, were estimated. The temperature dependence of magnetization (M vs. T) was also examined in the so-called zero-field-cooled (ZFC) and field-cooled (FC) conditions. The field strength applied was 0.01 T, and the experimental procedure was described in previous papers [17, 21, 26].

Morphological observations were performed using a field emission scanning electron microscope (FE-SEM), Hitachi S-4800. The samples were sputter coated with Pt before observation.

Wide-angle X-ray diffraction (WAXD) measurements were conducted using a Rigaku diffractometer, R-AXIS RAPID II. The apparatus was operated at 50 kV and 100 mA, and Ni-filtered CuKα radiation (0.154 nm) was utilized.

Evaluation of the macroscopic response behavior to an external magnetic field

For visual observation of the magnetic field response, larger specimens were prepared. For this purpose, a Car/PVA sol sample containing iron oxide at 65 °C was poured into a Teflon container (interior dimensions of 20 mm wide × 40 mm long × 10 mm deep), and 30 °C *t*-BuOH was gradually added into the vessel to form a gel. The gel sample was allowed to stand for 10 min in the *t*-BuOH bath, stretched to three times its original length using a hand-cranked drawing device in the air at 23 °C, and air-dried while attached to the drawing device to prepare a sheet specimen. The obtained samples were appropriately cut to size and used. Gels that were air-dried without being stretched were used as as-cast samples for reference. In addition, gels that were stretched and then cut without drying were subjected to observation as water-swollen Car/PVA/Fe specimens.

Several test pieces cut from the drawn sheets were utilized for observation of the macroscopic response behavior to an external magnetic field. The observation was performed by the following two methods: (1) The test pieces were floated on ethanol in a Petri dish, and a bar magnet of 0.15 T was employed for the field application. (2) A rectangular, water-swollen Car/PVA/Fe sample was cut so that the bottom was nearly square, and two different color tapes were affixed to the opposing side faces. A thread was attached to one end of the sample, and the entire sample was suspended, such that the DD was perpendicular to the gravitational field. A 0.15-T bar magnet was brought close

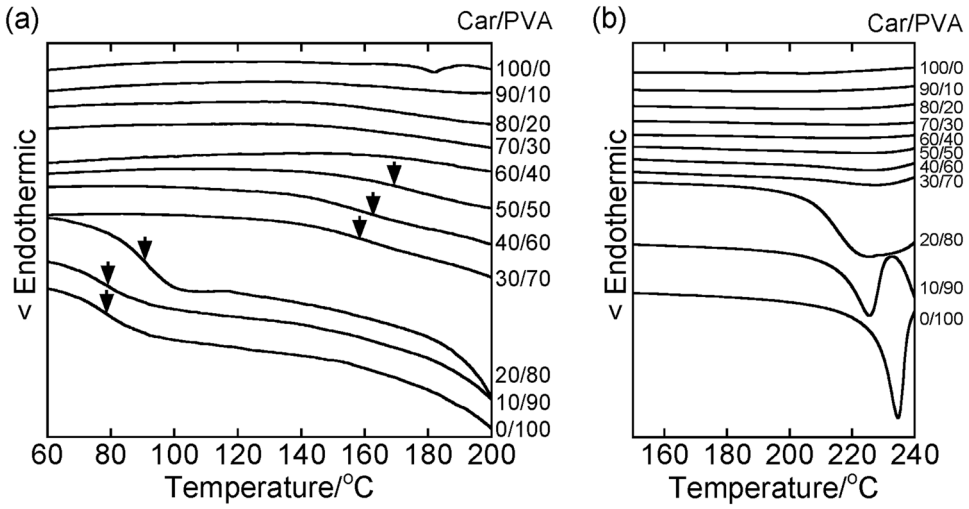

Fig. 1 DSC thermograms of the Car/PVA composites in the second heating scan. The midpoint T_g positions are indicated by arrows for the respective compositions illustrated in **a**. Part **b** represents the enlarged thermograms around the melting point of PVA

to the sample, and the movement of the sample was observed.

Results and discussion

In the present study, anionic Car was responsible for incorporating iron oxide nanoparticles and was combined with PVA, which shows an ability for high orientation. We thereby attempted to control the distribution of the magnetic iron oxide nanoparticles by stretching the entire nanocomposite to produce magnetically anisotropic materials.

To evaluate the compatibility of Car and PVA and determine an appropriate proportion, different compositions of Car/PVA were subjected to DSC measurements to detect possible variations in the glass transition temperature (T_g) with changing composition. The composites were prepared by solution casting from mixtures of the respective aqueous solutions. The DSC thermograms obtained in the second heating scan are shown in Fig. 1. As seen in Fig. 1a, the T_g values of Car alone and the Car-rich composites were unclear, but the T_g of the PVA component rose as the Car content increased. Based on such a systematic T_g shift, we concluded that there was good compatibility between the components in the amorphous regions of the composite series. For the PVA-rich composites (Car/PVA = 30/70–0/100), the melting point of PVA appeared at 200 °C or higher, as shown in Fig. 1b. Depression and broadening of the melting point were clearly observed as the Car content increased, and the crystalline domains of PVA disappeared in the Car-rich blends. This result is similar to the general behavior of amorphous/crystalline polymer pairs showing good compatibility. On the other hand, we found a gap in the T_g shift between 20 and 30 wt% Car. When the Car content was 20 wt% or less, it appeared that the physical properties, such as the thermal transition of the composites, were similar to those of PVA. Therefore, in the present study, the Car/PVA proportion was fixed at 20/80 by weight in anticipation of achieving high orientation in the nanocomposites and maximizing the iron oxide loading. The validity of selecting this composition will be demonstrated by the stretching behavior described below.

Based on the redox titration, the iron content was determined to be 9.2 wt% for the Car/PVA/Fe nanocomposite prepared by repeating the in situ synthesis of iron oxide three times. Because Car possesses sulfate groups, it was possible to prepare a composite in which iron ions were easily incorporated into the matrix, and the iron oxide particles were accommodated in large quantities.

In the drawing process, an aqueous sol-like sample (Car/PVA = 20/80 in weight) containing iron oxide was extruded from a micropipette into a *t*-BuOH bath to form a gel, and after a given amount of time, the gel was removed and stretched in the air. The optimum time for immersion of the gel in *t*-BuOH was 10 min. When the gel was stretched with tweezers, it could be extended to four times its original length. Preliminary experiments showed that the compositions containing more than 20% Car could not be deformed by more than 1.5 times; the κ-type of Car gives a highly elastic gel [24, 25]. Incidentally, other coagulation baths (methanol, ethanol, and 2-propanol) were also utilized, but *t*-BuOH was the most suitable based on the stretchability of the wet nanocomposites. This result may be attributable to the speed of coagulation; the coagulation rate of the present sample decreased in the order of methanol, ethanol, 2-propanol, and *t*-BuOH. Slower coagulation and precipitation in *t*-BuOH were also advantageous for maintaining the flexibility and deformability of the polymer network in the gel sample for a longer time. Thus, the Car/PVA/Fe nanocomposites could be easily stretched.

The samples subjected to the following various characterizations were the as-spun samples (via micropipette

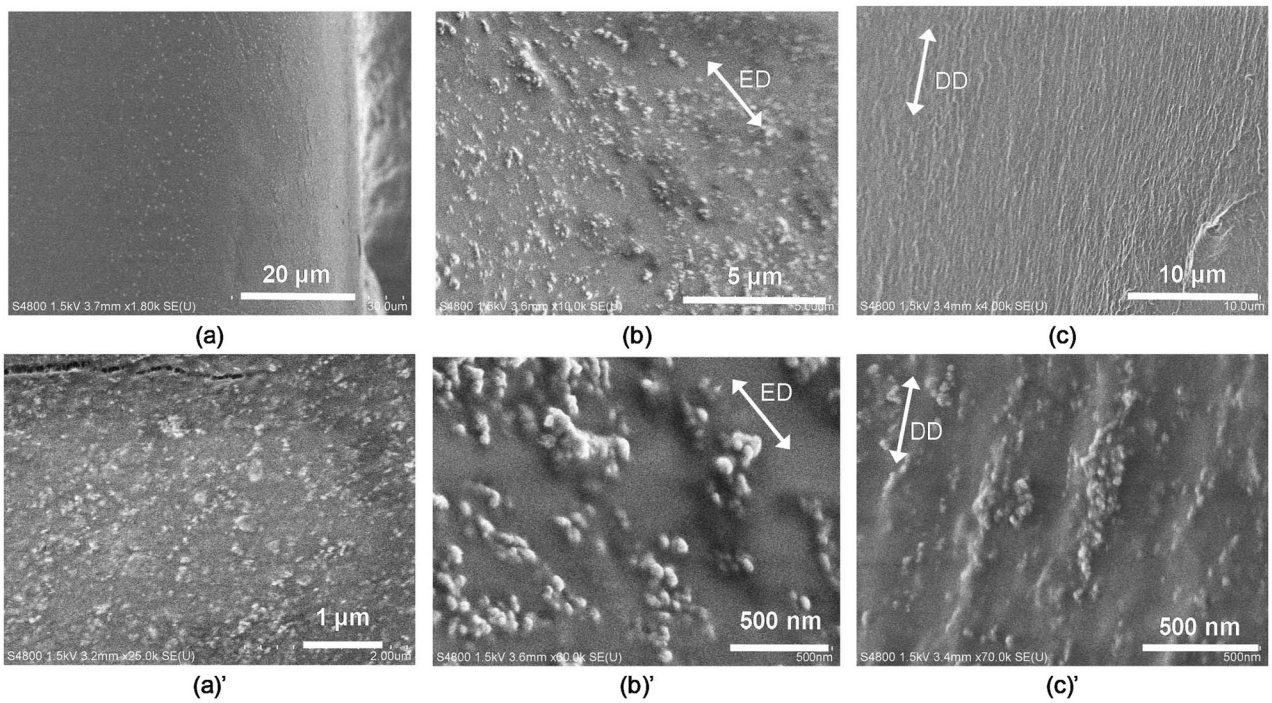

Fig. 2 FE-SEM images of the surfaces of **a** as-cast, **b** as-spun, and **c** drawn (fourfold) sheets of Car/PVA/Fe. The images labeled with a prime symbol are the enlarged views

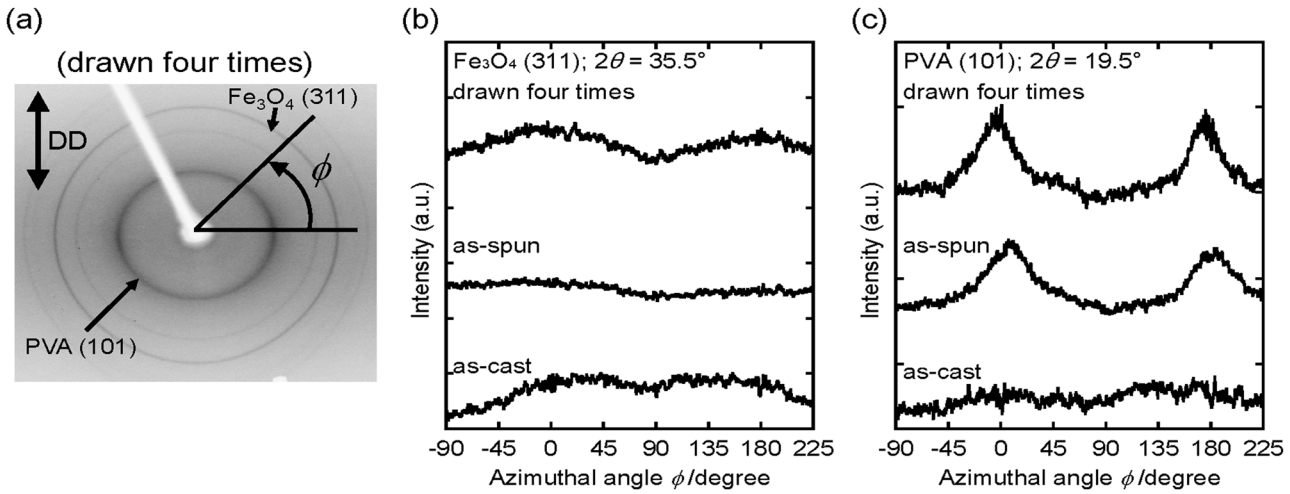

Fig. 3 WAXD results for the sheets of Car/PVA/Fe: **a** WAXD pattern of the sheet drawn to four times the original length, and azimuthal intensity profiles of the **b** Fe_3O_4 (311) and **c** PVA (101) diffractions for the as-cast, as-spun, and drawn (fourfold) sheets

extrusion) and those stretched with tweezers; each was air-dried with both ends fixed to a glass slide to form a nearly rectangular sheet. For comparison, we also show data for the as-cast sheets obtained by air drying the sol.

FE-SEM images of the surfaces of the as-cast, as-spun, and drawn samples are shown in Fig. 2. For the as-cast sample, granular particles of iron oxide were randomly dispersed, as shown in Fig. 2a. In contrast, the image in Fig. 2b indicates that iron oxide particles were distributed on the surface of the as-spun sample. The size of the particles estimated from the image was 50–100 nm, and these particles seemed to partially aggregate and slightly align along the extrusion direction (ED). With regard to the surface of the sample stretched to four times its original length (Fig. 2c), it was confirmed that the iron oxide particles were gathered and arranged along the drawing direction (DD) to form array structures (typically <1 μm length and <200 nm diameter). The diameters of the individual iron oxide

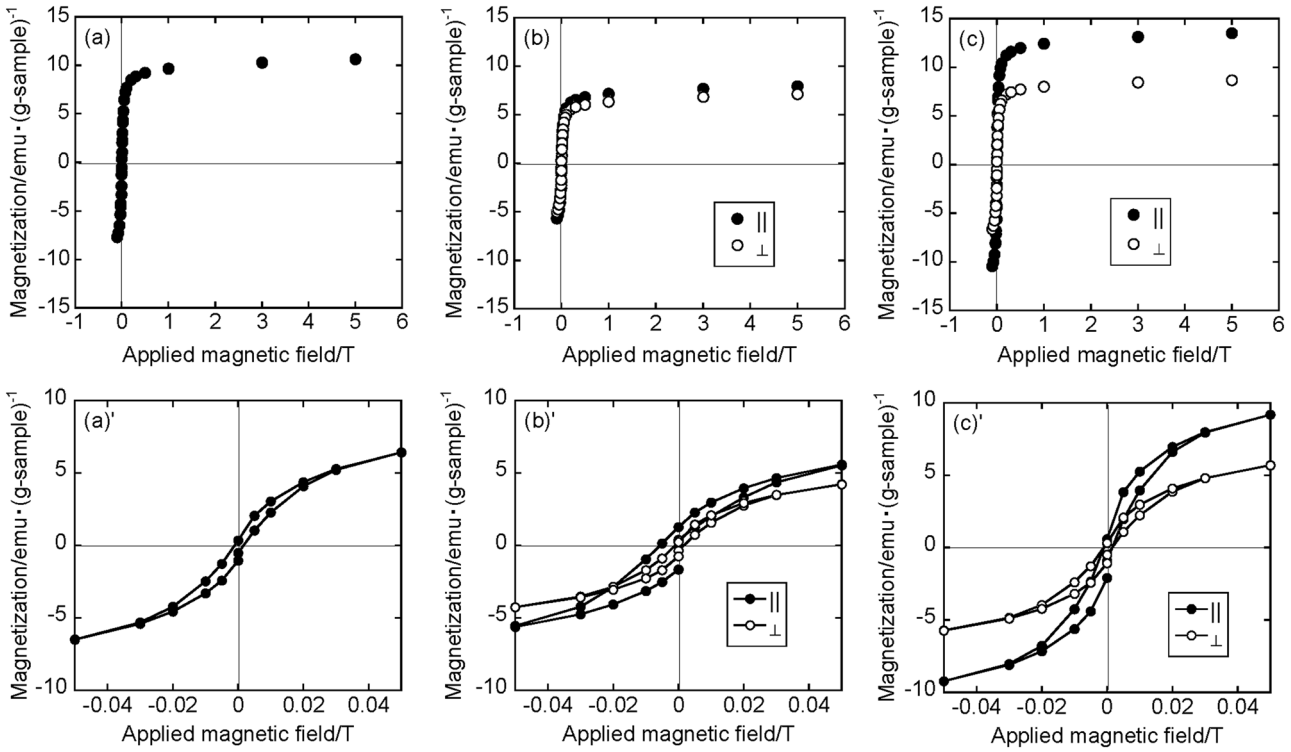

Fig. 4 Magnetization vs. applied field plots at 298 K for the **a** as-cast, **b** as-spun, and **c** drawn (fourfold) Car/PVA/Fe samples. The plots labeled with a prime symbol in **a–c** illustrate the data on an enlarged scale. Panels **b** and **c** include the magnetization data in two sets of the ED and DD parallel (||) and perpendicular (⊥) to the applied field

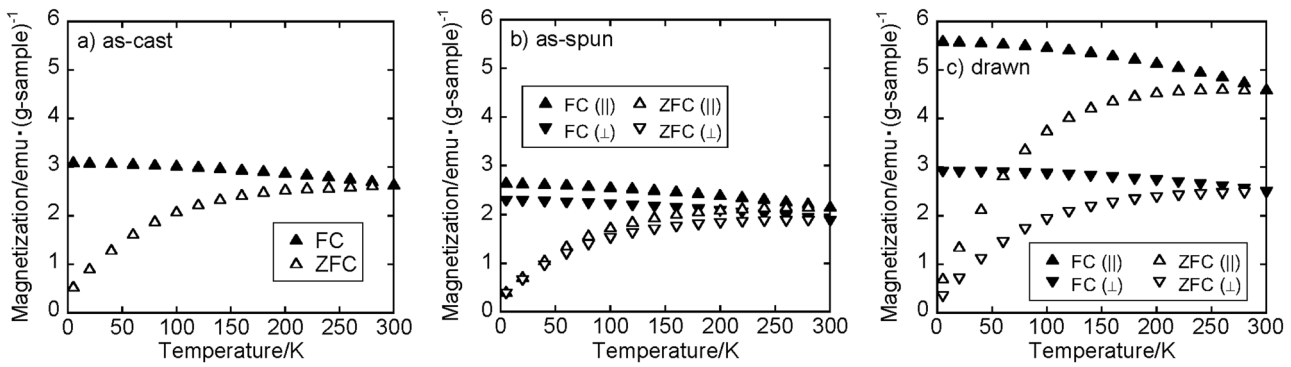

Fig. 5 Temperature dependence of the magnetization for the **a** as-cast, **b** as-spun, and **c** drawn (fourfold) samples examined with a field strength of 0.01 T in ZFC (open symbols) and FC (solid symbols) conditions. Panels **b** and **c** include the magnetization data in two sets of ED or DD parallel (||) and perpendicular (⊥) to the applied field

particles were 50–100 nm, as was the case in the as-spun specimen. For the drawn sample, a bundle-like morphology (<1 μm width) was also developed, seemingly exhibiting a fibrous orientation at low magnification.

Figure 3 illustrates the WAXD data for the sheets of Car/PVA/Fe. The DD and ED of the samples were set to be perpendicular to the equator of the WAXD pattern, as exemplified in Fig. 3a for the sheet drawn to four times the original length. The diagram was characterized by diffractions from two kinds of crystals, spinel ferrite of Fe_3O_4 and PVA, as indexed from several intense diffractions in the pattern. As shown in Fig. 3b, a slight preferential orientation was observed in the diffraction of the (311) plane of the iron oxide unit in the fourfold stretched sample, although the peak was broad. However, this peak was barely observable in the as-spun samples. With regard to the PVA crystals (Fig. 3c), the azimuthal scanning of the (101) diffraction at $2\theta = 19.5°$ showed no significant change in intensity for the as-cast sheet. The azimuthal profiles of the as-spun and drawn sheets, meanwhile, exhibited maxima at the equator

(azimuthal angles $\phi = 0$ and 180°). It was thus found that the PVA crystals in the as-spun sample preferentially oriented along the ED during extrusion from the micropipette and regeneration in the coagulation bath. When the sample was stretched, the peaks in the azimuthal scan became somewhat sharper. This suggests an improvement in the crystallinity and orientation in the drawing and drying processes, although it is necessary to further investigate the formation and growth of PVA crystals. Additionally, the orientation of the amorphous chains may have been improved as well.

SQUID magnetometry was conducted on the samples, and the effect of the structural anisotropy was evaluated. For the measurements, we used small, rectangular specimens cut from the oriented sheets with dimensions of 5 mm in the ED or DD direction and 2 mm in the direction perpendicular to the ED or DD. As-cast sheets cut into 2-mm squares were also provided for the measurements.

Figure 4 shows the magnetization (M) vs. applied field (H) plots at 298 K for the air-dried specimens. As seen in the enlarged plots ((a)′–(c)′), all of the samples imparted a perceptible hysteresis in the range of −0.05–0.05 T, from which the magnetism at this temperature was judged to be ferromagnetic (FM), although the extent of the hysteresis loop was generally small or moderate. We previously reported that similar FM behavior was observed at 100 K for parallel composites prepared by three repetitions of the in situ synthesis of iron oxide in matrices containing Car [17, 21]. To give FM behavior means that the size of each iron oxide particle is reasonably large. The magnetism was consistent with the observation of iron oxide particles with 50–100 nm diameters by FE-SEM.

Figure 5 illustrates the ZFC and FC curves obtained for the three samples in an applied field of 0.01 T. As seen in Fig. 5a, no clear maximum was observed in the ZFC curve for the as-cast sample. The FC and ZFC curves were close to each other at room temperature (300 K) but separated at slightly lower temperature, and the divergence became remarkable with decreasing temperature. The fact that the temperature at which the FC and ZFC curves separated was close to room temperature was consistent with the tendency of the composite to show FM at room temperature. The tendency remained nearly unchanged regardless of the processing route and M measuring direction, as seen from the data in Fig. 5b and 5c.

As for the influence of the orientation, the magnetization ($M_{\parallel}$) of the as-spun and drawn sheets in the parallel set was always larger than that ($M_{\perp}$) in the perpendicular set. This result indicates that the axis of easy magnetization lies parallel to the ED or DD of the sheets. The magnetic anisotropy, represented by the ratio $M_{\parallel}/M_{\perp}$, was generally higher in the drawn sample, particularly at lower-field strengths, when the samples were compared at a constant temperature of 298 K (see Table 1). In Fig. 5b and 5c, the ZFC and FC data for the two samples, each shown for both the parallel and perpendicular sets, demonstrate the anisotropy of magnetization at 0.01 T over a wide range of temperatures; the drawn sample is superior to the as-spun sample in the degree of the anisotropy.

Table 1 $M_{\parallel}/M_{\perp}$ at different magnetic fields obtained by SQUID magnetometry at 298 K

	$M_{\parallel}/M_{\perp}$		
	at 0.005 T	at 0.050 T	at 3 T
As-spun	1.15	1.13	1.12
Drawn	1.82	1.61	1.55

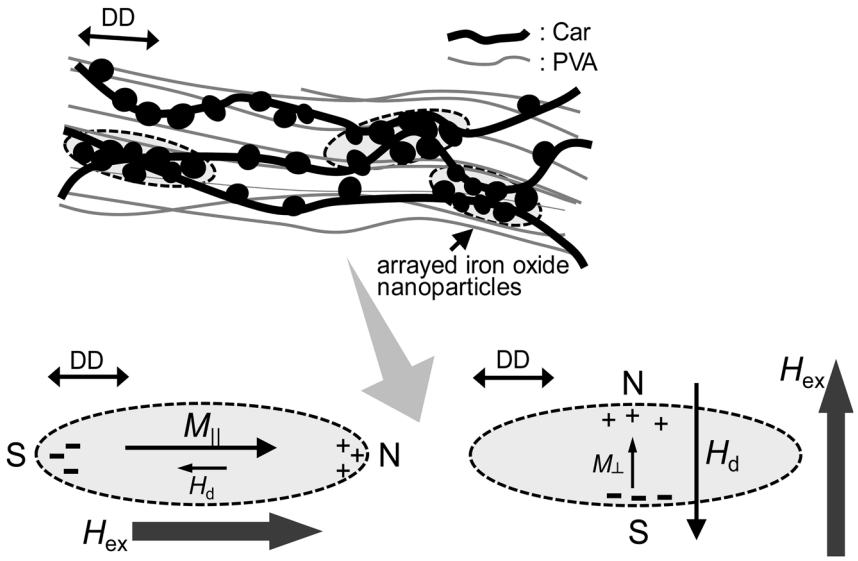

Fig. 6 Pictorial representation that models the oriented aggregates of iron oxide nanoparticles distributed in a drawn matrix composed of Car and PVA and the magnetic anisotropy derived from the anisotropic microstructure. The concept of this figure was reported in Fig. 9 of our previous paper [21]. (Rearranged with permission from ref. [21]: Copyright 2016 by Elsevier Ltd.)

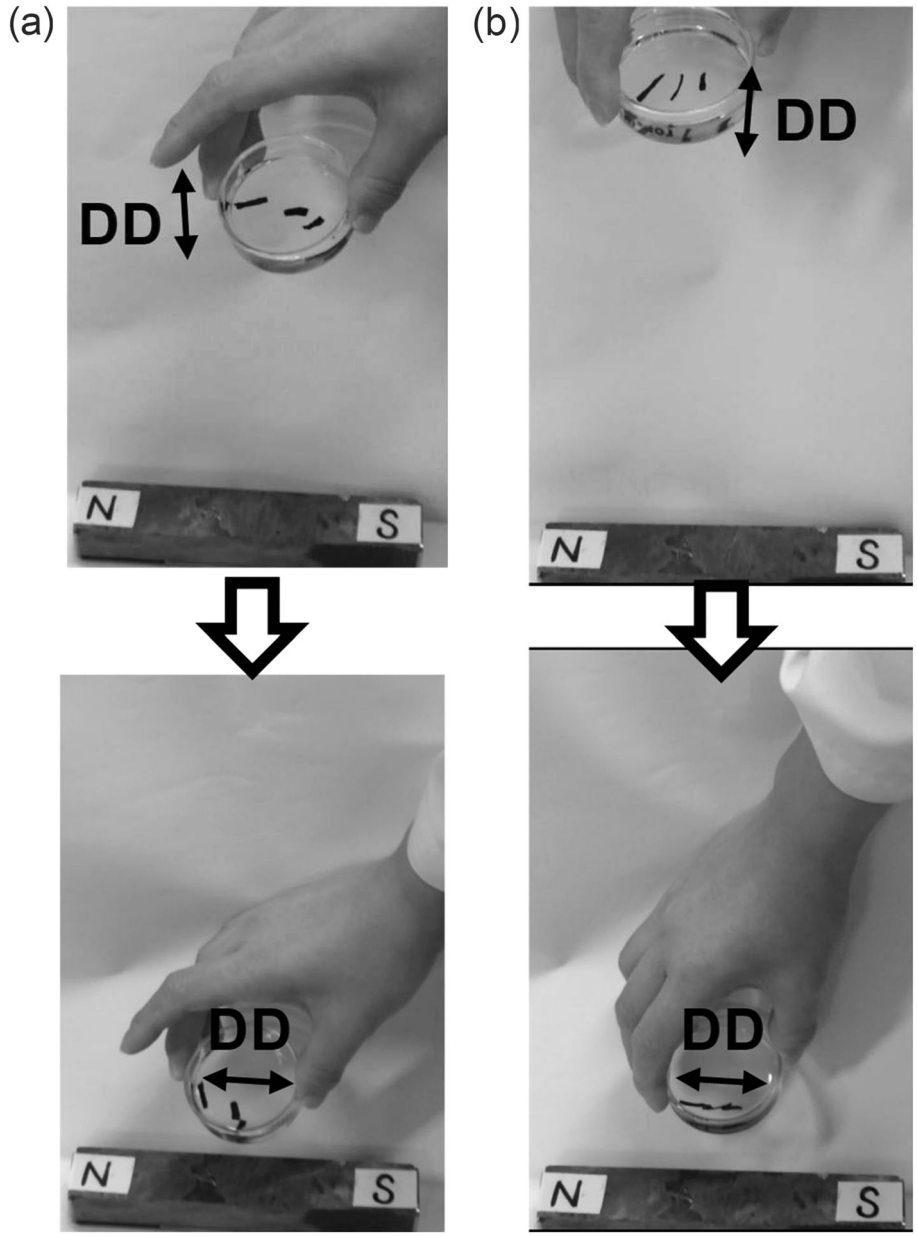

Fig. 7 Photographic data showing the magnetic orientation behavior of Car/PVA/Fe rectangular strips cut from a drawn sheet (draw ratio of three times) with the DD **a** perpendicular and **b** parallel to the longer axis of the strip. The strips were floated on ethanol in a glass dish. (Color figure online)

Concerning the magnetic anisotropy observed above, the anisotropy of the macroscopic shape of the samples likely partially contributed to the results because the specimens were cut so that the principal (longer) axis was in the DD or ED direction. Nevertheless, it should be noted that the drawn and as-spun specimens were cut into similar rectangular forms for the SQUID measurements. Here we consider the microscopic scale, i.e., the state of individual magnetic nanoparticles. Because we observed no substantial shape anisotropy and no explicit crystallite orientation for the iron oxide (Fe_3O_4) nanoparticles by FE-SEM and WAXD, respectively, each magnetic nanoparticle (approximately round) can be assumed to hardly show magnetic anisotropy. To interpret the above observation, we thus assumed that the distance between magnetic nanoparticles was small enough to allow the domain wall to move, and the nanoparticles formed a cluster following deformation of the polymer matrix. This aggregation would be significant in the drawn specimen, which showed a particularly high anisotropy of magnetization. Furthermore, the FE-SEM data (Fig. 2c) indicated that the iron oxide particles in the drawn sheet assembled to form an array along the DD. As modeled in Fig. 6, the individual aggregates can be regarded as oriented magnetic bodies of a prolate ellipsoid. When these bodies are subjected to an external field, H_{ex}, a so-called demagnetizing field, H_d, is induced inside the bodies in the direction opposite to H_{ex}; the intensity of H_d is stronger along the shorter axis than the

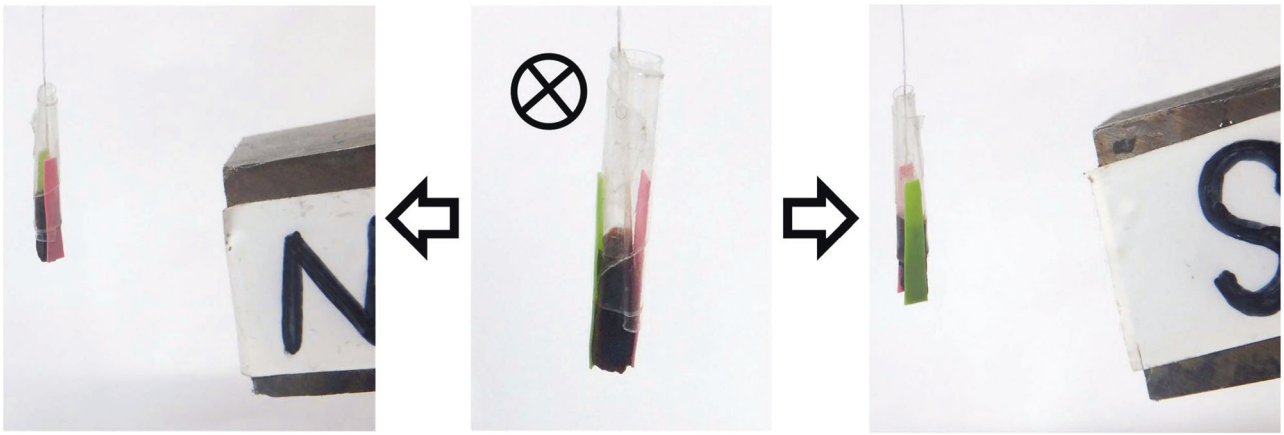

Fig. 8 Response of a Car/PVA/Fe drawn sample swollen with water to a bar magnet. The gel sample was suspended in the vertical direction. The bottom surface of the sample was essentially square. As shown in the middle figure, the sample was first positioned so that the DD was perpendicular to this page

longer axis of the ellipsoid [27]. This results in anisotropy ($M_{\parallel} > M_{\perp}$) in the magnetization, which is expressed as $M = \chi(H_{ex} - H_d)$ with susceptibility χ.

The formation of such oriented elliptical magnetic bodies was more clearly supported by visual observation of the response of the drawn (three times) sample as a whole to an external magnetic field. Figure 7 illustrates the observations for rectangular test pieces cut from a drawn sheet. The longer axes of the strips were perpendicular (Fig. 7a) or parallel (Fig. 7b) to the DD. The samples were floated on ethanol in a Petri dish. When the Petri dish was brought close to a bar magnet (0.15 T), the strips rotated so that the DD and the force lines of the magnet were parallel to each other, regardless of the cutting directions.

As a control experiment, the magnetic field response was similarly evaluated for the as-cast samples as well. When the in-plane aspect ratio was ~1, the as-cast samples did not rotate but were attracted to the magnet. For rectangular shapes, however, the cast samples uniformly moved so that the longer axes were invariably parallel to the magnetic flux lines.

The different magnetic responses observed above for the nanocomposite sheets are interpretable in terms of an effect of the shape anisotropy [27]. However, the dimensional scale of the anisotropy and therefore the structural factor varied substantially between the drawn sheet and the as-cast one. In the drawn sheets, the loaded iron oxide nanoparticles were assembled in larger aggregates (typically <1 μm length and <200 nm diameter) to form an array along the DD. As modeled in Fig. 6, the individual aggregates can be regarded as oriented magnetic bodies of a prolate ellipsoid. On the other hand, the as-cast sheet had no preferred arrangement of the granular iron oxide nanoparticles. In this situation, only the macroscopic shape itself is a source of magnetic anisotropy. Therefore, when the as-cast sheet was cut into rectangular strips, the longer axes became the easy axis of magnetization. For the strips of the drawn sheet, however, it is reasonable to conclude that the shape anisotropy in the microstructure rather than that of the entire sample more strongly contributed to the anisotropy of the material magnetization. This principle was manifested in the magnetic orientation behavior (Fig. 7a) of the strips in which the longer axis was cut perpendicular to the DD.

Another magnetic response experiment enabled us to further confirm the microscopic magnetic anisotropy of our oriented samples. As shown in the middle of Fig. 8, we suspended a water-swollen Car/PVA/Fe specimen with a square basal plane, such that the DD was perpendicular to the plane of the paper. When a bar magnet was brought close to the sample, the specimen rotated, and the DD and magnetic force became parallel. If the N and S poles of the magnet were exchanged, the specimen rotated in the opposite direction. Because the bottom of the sample was nearly square and there was no influence of anisotropy due to the shape of the whole sample, the effect of the microscopic magnetic anisotropy in the drawn sample was more clearly confirmed. If the sample DD was in the vertical direction, namely, perpendicular to the force lines of the magnet, the sample was simply attracted to the magnet without rotating.

In extension of these results, we can make a variety of orientation patterns of strips in a static magnetic field by cutting strips at various angles relative to the DD from the drawn nanocomposites. From a more practical standpoint, the drawn nanocomposites explored here serve as an example of functional materials that can provide magneto-responsive microchips of <100 μm, each having a prescribed axis of orientation; the chips would be applicable to a micro-patterning element controlled by a magnetic force.

Conclusion

Magnetic iron oxide nanoparticles were synthesized in situ in a compatible Car/PVA polymer matrix. By stretching the obtained magnetic nanocomposite in the gel state, the iron oxide nanoparticles loaded inside formed approximately elliptical magnetic clusters. As a result, we succeeded in making the composites anisotropically responsive to an external magnetic field. Here, Car and PVA were responsible for coordinating to iron and achieving a high orientation, respectively, in the nanocomposites. These constituents are industrially common raw materials, and the preparation process for the nanocomposites was simple. Although the magnetic iron oxide nanoparticles accommodated in the composites were granular and did not show a remarkable anisotropic magnetization by themselves, microscopic rearrangement was successfully accomplished to impart macroscopic magnetization anisotropy. We believe that this method can be practically applied to easily obtain magnetically anisotropic materials.

Acknowledgments We acknowledge Dr A. Otsuka of the Research Center for Low Temperature and Materials Science, Kyoto University, for his technical support in the SQUID magnetometry measurements. This work was partially financed by a Grant-in-Aid for Scientific Research (A) (No. 26252025 to Y.N. and No. 17H01480 to Y.T.) from the Japan Society for the Promotion of Science and by the Environment Research and Technology Development Fund (3K153010 to Y.T.) of the Ministry of the Environment, Japan.

References

1. Marchessault RH, Ricard S, Rioux P. *In situ* synthesis of ferrites in lignocellulosics. Carbohydr Res. 1992;224:133–9.
2. Raymond L, Revol JF, Marchessault RH, Ryan DH. *In situ* synthesis of ferrites in ionic and neutral cellulose gels. Polymer. 1995;36:5035–43.
3. Kroll E, Winnik FM, Ziolo RF. *In situ* preparation of nanocrystalline γ-Fe_2O_3 in iron(II) cross-linked alginate gels. Chem Mater. 1996;8:1594–6.
4. Sourty E, Ryan DH, Marchessault RH. Characterization of magnetic membranes based on bacterial and man-made cellulose. Cellulose. 1998;5:5–17.
5. Veiga V, Ryan DH, Sourty E, Llanes F, Marchessault RH. Formation and characterization of superparamagnetic cross-linked high amylose starch. Carbohydr Polym. 2000;42:353–7.
6. Jones F, Cölfen H, Antonietti M. Interaction of kappa-carrageenan with nickel, cobalt, and iron hydroxides. Biomacromolecules. 2000;1:556–63.
7. Suber L, Foglia S, Ingo GM, Boukos N. Synthesis, and structural and morphological characterization of iron oxide-ion-exchange resin and -cellulose nanocomposites. Appl Organomet Chem. 2001;15:414–20.
8. Chatterjee J, Haik Y, Chen CJ. Biodegradable magnetic gel: Synthesis and characterization. Colloid Polym Sci. 2003;281:892–6.
9. Nishio Y, Yamada A, Ezaki K, Miyashita Y, Furukawa H, Horie K. Preparation and magnetometric characterization of iron oxide-containing alginate/poly(vinyl alcohol) networks. Polymer. 2004;45:7129–36.
10. Si S, Kotal A, Mandal TK, Giri S, Nakamura H, Kohara T. Size-controlled synthesis of magnetite nanoparticles in the presence of polyelectrolytes. Chem Mater. 2004;16:3489–96.
11. Daniel-da-Silva AL, Trindade T, Goodfellow BJ, Costa BFO, Correia RN, Gil AM. In situ synthesis of magnetite nanoparticles in carrageenan gels. Biomacromolecules. 2007;8:2350–7.
12. Matsumoto Y, Teramoto Y, Nishio Y. Preparation of thermoplastic magnetic wood via etherification and *in-situ* synthesis of iron oxide. J Wood Chem Technol. 2010;30:373–81.
13. Olsson RT, Azizi Samir MAS, Salazar-Alvarez G, Belova L, Ström V, Berglund La, Ikkala O, Nogués J, Gedde UW. Making flexible magnetic aerogels and stiff magnetic nanopaper using cellulose nanofibrils as templates. Nat Nanotechnol. 2010;5:584–8.
14. Li G, Du Y, Tao Y, Deng H, Luo X, Yang J. Iron(II) cross-linked chitin-based gel beads: preparation, magnetic property and adsorption of methyl orange. Carbohydr Polym. 2010;82:706–13.
15. Liu S, Zhou J, Zhang L. In situ synthesis of plate-like Fe_2O_3 nanoparticles in porous cellulose films with obvious magnetic anisotropy. Cellulose. 2011;18:663–73.
16. Katepetch C, Rujiravanit R. Synthesis of magnetic nanoparticle into bacterial cellulose matrix by ammonia gas-enhancing in situ co-precipitation method. Carbohydr Polym. 2011;86:162–70.
17. Oya K, Tsuru T, Teramoto Y, Nishio Y. Nanoincorporation of iron oxides into carrageenan gels and magnetometric and morphological characterizations of the composite products. Polym J. 2013;45:824–33.
18. Zhou J, Li R, Liu S, Li Q, Zhang L, Zhang L, Guan J. Structure and magnetic properties of regenerated cellulose/Fe_3O_4 nanocomposite films. J Appl Polym Sci. 2009;111:2477–84.
19. Nypelö T, Rodriguez-Abreu C, Rivas J, Dickey MD, Rojas OJ. Magneto-responsive hybrid materials based on cellulose nanocrystals. Cellulose. 2014;21:2557–66.
20. Nypelö T, Rodriguez-Abreu C, Kolena'ko YV, Rivas J, Rojas OJ. Microbeads and hollow microcapsules obtained by self-assembly of Pickering magneto-responsive cellulose nanocrystals. ACS Appl Mater Interfaces. 2014;6:16851–8.
21. Yoshitake H, Sugimura K, Teramoto Y, Nishio Y. Magnetic property of oriented films of cellulose nanocrystal/carrageenan composites containing iron oxide nanoparticles: effect of anisotropic aggregation of the nanoparticles. Polymer. 2016;99:147–56.
22. Tanaka T, Lu T, Yuasa S, Yamaura K. Structure and properties of poly(vinyl alcohol)/κ-carrageenan blends. Polym Int. 2001;50:1103–8.
23. Mahdavinia GR, Massoudi A, Baghban A, Shokri E. Study of adsorption of cationic dye on magnetic kappa-carrageenan/PVA nanocomposite hydrogels. J Environ Chem Eng. 2014;2:1578–87.
24. Nishinari K. Longitudinal vibrations of high-elastic gels as a method for determining viscoelastic constants. Jpn J Appl Phys. 1976;15:1263–70.
25. Hossain KS, Nemoto N, Nishinari K. Dynamic viscoelasticity of iota carrageenan gelling system near sol-gel transition. Nihon Reoroji Gakkaishi (J Soc Rheol Jpn). 1997;25:135–42.
26. Gittleman JI, Abeles B, Bozowski S. Superparamagnetism and relaxation effects in granular Ni-SiO_2 and Ni-Al_2O_3 films. Phys Rev B. 1974;9:3891–7.
27. Cullity, BD & Graham, CD. Introduction to magnetic materials, 2nd ed. (New York: John Wiley & Sons; 2011).